Journal of Power Sources 257 (2014) 280–285

Contents lists available at ScienceDirect

Journal of Power Sources

journal homepage: www.elsevier.com/locate/jpowsour

High rate capability core–shell lithium titanate@ceria nanosphere anode material synthesized by one-pot co-precipitation for lithium-ion batteries

Xinjie Yang [a], Yudai Huang [a,*], Xingchao Wang [a], Dianzeng Jia [a,*], Wei Kong Pang [b,c], Zaiping Guo [b], Xincun Tang [a]

[a] Key Laboratory of Material and Technology for Clean Energy, Ministry of Education, Key Laboratory of Advanced Functional Materials, Autonomous Region, Institute of Applied Chemistry, Xinjiang University, Urumqi 830046, Xinjiang, China
[b] School of Mechanical, Materials, and Mechatronic Engineering, Institute for Superconducting & Electronic Materials, Faculty of Engineering, University of Wollongong, NSW 2522, Australia
[c] Australian Nuclear Science and Technology Organisation, Locked Bag 2001, Kirrawee DC, NSW 2232, Australia

HIGHLIGHTS

- $Li_4Ti_5O_{12}$@CeO_2 nanosphere was synthesized by a one-pot co-precipitation method.
- CeO_2 layer enhances the electronic conductivity and lithium ion diffusivity in $Li_4Ti_5O_{12}$.
- $Li_4Ti_5O_{12}$@CeO_2 nanosphere exhibits excellent rate capability and cycling stability.

ARTICLE INFO

Article history:
Received 9 December 2013
Received in revised form
13 January 2014
Accepted 1 February 2014
Available online 11 February 2014

Keywords:
High rate capability
Core–shell
Lithium titanate
Ceria
Lithium-ion batteries

ABSTRACT

Core–shell $Li_4Ti_5O_{12}$@CeO_2 nanosphere has been synthesized by a one-pot co-precipitation method. The structure and morphology of the as-prepared materials have been analyzed by X-ray diffraction and transmission electron microscopy. The results show that CeO_2 is successfully coated on the surface of the $Li_4Ti_5O_{12}$ besides partial doping of Ce^{4+} into the $Li_4Ti_5O_{12}$ structure. The $Li_4Ti_5O_{12}$@CeO_2 nanosphere exhibits excellent capacity of 152 mAh g^{-1} even after 180 cycles at 10 C, with no noticeable capacity fading. Furthermore, the sample shows much improved rate capability at 40 C compared with pure $Li_4Ti_5O_{12}$ when used as anode material for lithium-ion batteries. The introduction of CeO_2 enhances not only the electric conductivity of $Li_4Ti_5O_{12}$, but also the lithium ion diffusivity in $Li_4Ti_5O_{12}$, resulting in significantly improved electrochemical performance of the $Li_4Ti_5O_{12}$.

1. Introduction

It is well known that lithium-ion batteries (LIBs) have higher energy density, suitable design for portable applications, and longer lifetimes than comparable battery technologies [1]. Graphite-based materials have been generally applied as anode materials in LIBs for many portable electric devices [2]. However, these LIBs containing graphite-based anodes suffer from safety problems [3]. There have been ongoing research efforts to search for alternative materials to carbonaceous anodes. Among the variety of alternative materials, spinel lithium titanate ($Li_4Ti_5O_{12}$) has drawn extensive attention as one of the most promising anode material candidates for LIBs [4], due to its advantageous features compared with conventional graphite-based anodes. $Li_4Ti_5O_{12}$ offers a flat voltage plateau close to 1.55 V (vs. Li^+/Li), which is beyond the reduction potential of most organic electrolytes, so that the formation of solid electrolyte interphase (SEI) could be avoided, which offers a great improvement in safety [5,6]. Furthermore, spinel $Li_4Ti_5O_{12}$ is a zero-strain insertion material, which exhibits negligible volume change during the Li^+ insertion/desertion processes, resulting in excellent cycling performance [7]. What's more,

* Corresponding authors. Tel./fax: +86 991 8588209.
E-mail addresses: huangyd@xju.edu.cn, hyd60045@163.com (Y. Huang), jdz@xju.edu.cn (D. Jia).

http://dx.doi.org/10.1016/j.jpowsour.2014.02.005
0378-7753/

the thermal stability plays an important role in the safety of LIBs, the high thermodynamic stability of spinel $Li_4Ti_5O_{12}$ is better appropriate for application in high power energy storage [8]. The low electrical and ionic conductivity of $Li_4Ti_5O_{12}$ can lead to poor high rate performance, however, that hinders its commercial application [9,10]. In an attempt to overcome this serious drawback, many strategies have been applied to improve the high rate capability of $Li_4Ti_5O_{12}$, including enhancement of its electric conductivity by doping with foreign atoms [11–21], synthesis of nanostructured $Li_4Ti_5O_{12}$ materials with various morphologies [22–25], and/or surface coating with a more conductive material [26,27]. Cheng et al. [27] prepared carbon-coated nanostructured $Li_4Ti_5O_{12}$ through the chemical vapor decomposition method combined with solid-state reaction. Zhu et al. [28] synthesized carbon-coated nanosized $Li_4Ti_5O_{12}$ by treating TiO_2 and sugar at 600 °C for 5 h under flowing N_2, and then combined it with a spray drying method, followed by annealing the products at 800 °C for 10 h under flowing N_2. Li et al. [29] prepared N-doped carbon coated $Li_4Ti_5O_{12}$ by a complex solution method. Carbon-based coatings can enhance the electric conductivity and promote charge transfer reactions, and this method has been successfully used to improve the rate capability of $Li_4Ti_5O_{12}$. Due to the complex preparation procedures, however, great efforts have also spent on other alternative coatings in order to achieve excellent rate performance and cycling stability.

Due to the direct and fast transformation between Ce (III) and Ce (IV), ceria (CeO_2) has good electrical conductivity and is one of the more favorable anode candidates for LIBs [30–33]. CeO_2 has already been used as a coating material for improving the electrochemical performance of cathode materials, such as in $LiCoO_2$ and $LiMn_2O_4$ electrodes [34,35]. To the best of our knowledge, however, there have been no reports on CeO_2-coated $Li_4Ti_5O_{12}$ composite as yet.

In this work, core–shell $Li_4Ti_5O_{12}$@CeO_2 nanosphere was prepared by a one-pot co-precipitation method, and the electrochemical performance and structure of the sample was systematically investigated. The results show that CeO_2 is successfully coated on the surface of the $Li_4Ti_5O_{12}$ besides partial doping of Ce^{4+} into the $Li_4Ti_5O_{12}$ structure. In addition, the $Li_4Ti_5O_{12}$@CeO_2 composite exhibits excellent cycling stability at the high rate of 10 C and outstanding rate capability, which are much improved relative to pure $Li_4Ti_5O_{12}$. Compared with the other coated $Li_4Ti_5O_{12}$ composites [28,29], the $Li_4Ti_5O_{12}$@CeO_2 composite shows even better rate performance. Moreover, our fabrication method is simple and can be easily scaled up, the facile one-pot synthesis would have better potential in future mass production than the commonly applied complicated coating procedures.

2. Experimental

2.1. Synthesis

The core–shell $Li_4Ti_5O_{12}$@CeO_2 nanosphere was synthesized by a one-pot co-precipitation procedure. Typically, 12 mL of tetrabutyl titanate was thoroughly mixed in ethanol to form a faint yellow homogeneous solution. Then, 1.208 g $LiOH\cdot H_2O$ and 0.1525 g $Ce(NO_3)_3\cdot 6H_2O$ were thoroughly dissolved in deionized water, by being slowly dropped into the yellow solution under vigorous stirred. The yellow transparent solution gradually turned into a white suspension. The mixture was stirred for 24 h, and then dried at 100 °C to fully remove the solvent, with subsequent heating to 600 °C for 5 h in air. Excess Li was used to compensate for the volatilization of Li at high temperature. The product was denoted as LTO-CR. For comparison, pure $Li_4Ti_5O_{12}$ material, which was denoted as LTO, was prepared by the same procedure without the addition of $Ce(NO_3)_3\cdot 6H_2O$.

2.2. Structural characterization

The crystal structures of the two samples were examined by X-ray diffraction (XRD: Bruker D8 Advance equipped with Cu Kα radiation). The morphologies of the two samples were characterized by transmission electron microscopy (TEM: H-600, Hitachi, Japan). Rietica ver. 1.77 [36] was employed to perform Rietveld analysis of the XRD data of the two samples. The optimized parameters included the background coefficients, zero-shift, peak shape parameters, phase of the lattice, oxygen positional parameters, and isotropic atomic displacement parameters. The figures of merit for the refinement included the Bragg statistical reliability factor (R_B) and the weighted profile factor (R_{wp}).

2.3. Electrochemical characterization

The working electrodes were prepared by first making the anode slurry by thoroughly mixing the active material, acetylene black, and poly (vinylidene fluoride) at a weight ratio of 75:15:10 in *N*-methyl pyrrolidinone solvent. The mixture was pasted on pure Cu foil and dried at 110 °C in a vacuum oven for 12 h. Coin-type cells (2032) were assembled with a solution of 1 M $LiPF_6$ in a 1:1 (volume ratio) mixture of ethylene carbonate and dimethyl carbonate as the electrolyte, a Celgard 2300 microporous polyethylene membrane as the separator, and a lithium disk as the counter electrode. All the cells were assembled in an argon-filled glove box, where the water and oxygen concentrations were kept at less than 5 ppm. Charge–discharge tests were carried out using a battery test system (CT2001A, Land, China) in the voltage range of 1.0–3.0 V (vs. Li^+/Li). Cyclic voltammograms (CVs) were collected in the voltage range of 1.0–3.0 V using a CHI660D electrochemical workstation with a scan rate of 0.1 mV s^{-1}. Electrochemical impedance spectroscopy (EIS) was conducted on a Zahner Elektrik electrochemical workstation in the frequency range of 10^{-1}–10^5 Hz, with an applied DC potential that was equal to the open circuit voltage of the cell and an AC oscillation of 5 mV. All the electrochemical tests were carried out at room temperature.

3. Results and discussion

XRD patterns for LTO and LTO-CR are shown in Fig. 1, in which the XRD peaks of CeO_2 are denoted by (*). All the diffraction peaks

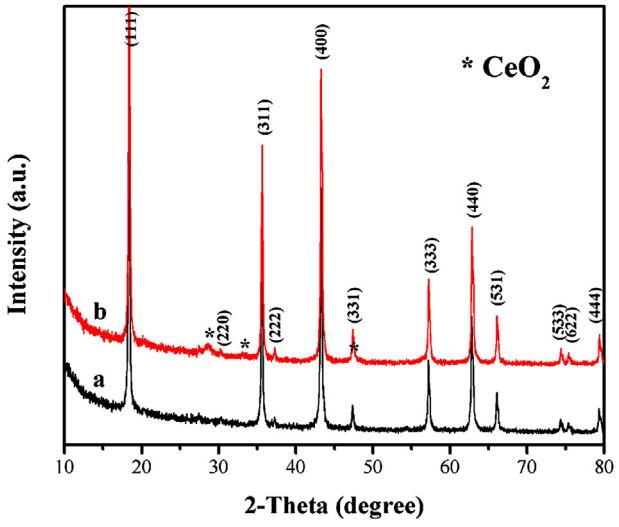

Fig. 1. XRD patterns of the as-prepared materials (a: LTO, b: LTO-CR).

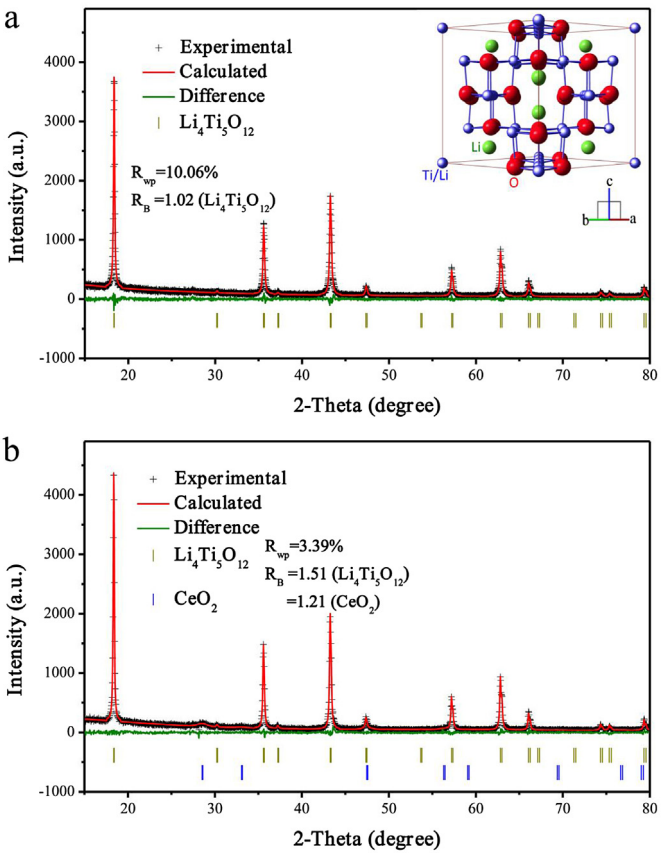

Fig. 2. Rietveld-refined fits using XRD data of (a) LTO and (b) LTO-CR. The inset to (a) shows the $Li_4Ti_5O_{12}$ unit cell.

of LTO can be readily indexed to the spinel $Li_4Ti_5O_{12}$ phase (space group $Fd\bar{3}m$, JCPDS Card No. 49-0207) [23], and no obvious impurity phase can be detected. The XRD pattern of LTO-CR is assigned to two crystalline phases, corresponding to standard data for spinel $Li_4Ti_5O_{12}$ (JCPDS No. 49-0207) and CeO_2 (JCPDS No. 34-0394) [30].

Fig. 2 shows the refinement plots based on the XRD data of the $Li_4Ti_5O_{12}$ samples, starting from a previously-published structural model – a cubic structure with space group $Fd\bar{3}m$ [37,38]. It is found that the pristine $Li_4Ti_5O_{12}$ has a smaller lattice parameter of 8.3578(6) Å than that of CeO_2-coated one (8.3622(2) Å). In addition, a small amount of CeO_2 ($Fm\bar{3}m$, 1.6(1) wt.%) was also detectable in the CeO_2-coated sample. The smaller detected amount of CeO_2 may suggest that Ce^{4+} ions are partially substituted into the $Li_4Ti_5O_{12}$ structure, and hence expand the lattice due to the larger ionic radius of Ce^{4+} (coordinate number (CN) = 6, 0.87 Å), which is larger than the corresponding radii for Ti^{4+} (CN = 6, 0.61 Å) and Li^+ (CN = 6, 0.76 Å). Moreover, the 32*e*-site oxygen position of pristine $Li_4Ti_5O_{12}$ is 0.23822 ($x = y = z$), whereas that of the coated sample is 0.23712(1). From this point of view, in comparison, the Coulombic attraction between Ti (Ce) and O is smaller in the pristine sample, but larger in the coated sample, suggesting better lithium diffusivity (weaker Li–O bonding) in the coated sample.

Fig. 2(b) contains the laboratory XRD pattern of the as-prepared $Li_4Ti_5O_{12}$@CeO_2 composite, together with the profile that was fitted using the $Fd\bar{3}m$ structure for $Li_4Ti_5O_{12}$ and the $Fm\bar{3}m$ structure for CeO_2. The crosses (+) represent the experimental data, the red solid-line is the calculated pattern, the green line is the difference between the experimental data and the calculated pattern, and the yellow and blue bars at the bottom show the Bragg positions of the reflections.

Fig. 3 presents TEM images of LTO and LTO-CR. It can be seen from Fig. 3(a) that the morphology of LTO is irregular and aggregated seriously. When the CeO_2 is coated on LTO, the morphology of the particles becomes spherical and less agglomeration (as shown in Fig. 3(b)). Spheres with the size ranging from 40 nm to 140 nm, and the thickness of CeO_2 on the surface of the $Li_4Ti_5O_{12}$ particles is around 8–15 nm. The results show that the formation of CeO_2 inhibits the aggregation of the $Li_4Ti_5O_{12}$ particles, to facilitate the formation of core–shell $Li_4Ti_5O_{12}$@CeO_2 nanosphere. Spherical morphology has advantageous features with packing efficiencies and high volumetric specific energy, which has promising in commercial applications [39].

Fig. 4 shows CVs of the LTO and LTO-CR. The CVs of both samples show one pair of redox peaks, but compared with the LTO, the current peaks of the LTO-CR are much higher. The redox peaks at about 1.67/1.43 V for LTO and 1.66/1.49 V for LTO-CR correspond to the two-phase charge–discharge reaction of the Ti^{3+}/Ti^{4+} redox couple [40,41]. The potential difference between the anodic and cathodic peaks for the LTO-CR relative to the LTO electrode decreases from 0.24 to 0.17 V. This decrease in potential difference can be ascribed to the effective electrical conductivity in the CeO_2 layer [32] and better lithium diffusivity (weaker Li–O bondings) in the coated sample. In addition, the redox peaks at about 1.30/1.20 V for CeO_2 are not detectable [42], possibly due to the low content of CeO_2 (1.6(1) wt.% in the composite). The CeO_2 coating did not

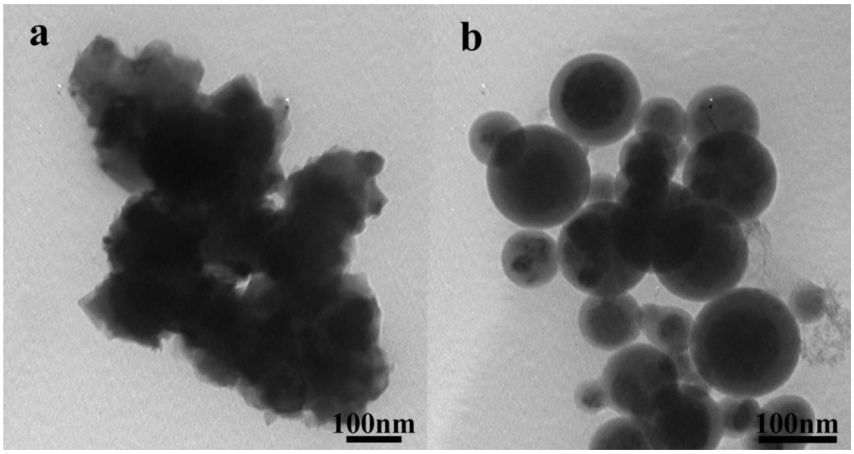

Fig. 3. TEM images of the as-prepared materials: (a) LTO, (b) LTO-CR.

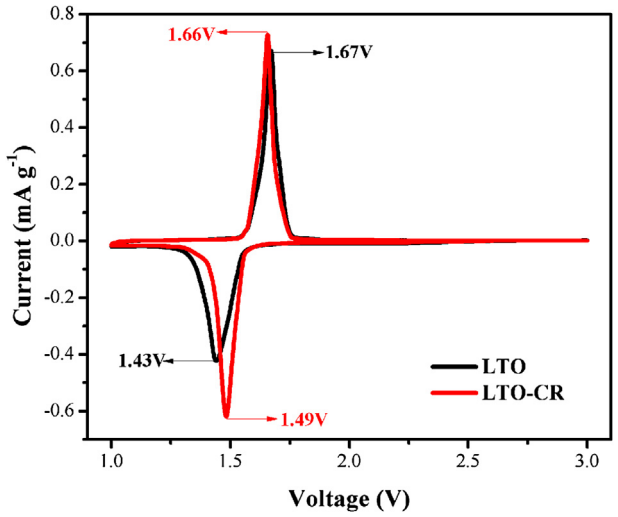

Fig. 4. Cyclic voltammograms of LTO and LTO-CR.

change the intrinsic properties of $Li_4Ti_5O_{12}$ in this voltage range, but it does produce good electrical contact that facilitates charge transfer [34].

Fig. 5 displays the charge–discharge voltage profiles of LTO and LTO-CR at 0.2 C (at the first cycle). Similar to LTO, the charge and discharge curves of LTO-CR show only one clear plateau. The initial discharge capacity of the LTO-CR is 186.6 mAh g^{-1} at 0.2 C, which is higher than that of LTO (173.3 mAh g^{-1}), and even higher than the theoretical capacity of spinel $Li_4Ti_5O_{12}$ (175 mAh g^{-1}). Bai et al. [13] and Yi et al. [16] reported that the increased capacity may be attributed to lattice distortion induced by the substitution of doped ions for Ti^{4+} and/or Li^+. Rietveld analysis of XRD data in this work illustrates the partial Ce^{4+} dope into the $Li_4Ti_5O_{12}$ structure, expand the lattice due to the larger ionic radius of Ce^{4+} (coordinate number (CN) = 6, 0.87 Å), which is larger than the corresponding radii for Ti^{4+} (CN = 6, 0.61 Å) and Li^+ (CN = 6, 0.76 Å). The substitution of Ce^{4+} may be responsible for increasing of the initial capacity of the LTO-CR. Furthermore, the inset presents the voltage difference between the charge and discharge plateaus. It can be seen that the ΔV of the LTO-CR (27 mV) is smaller than that of LTO (35 mV),

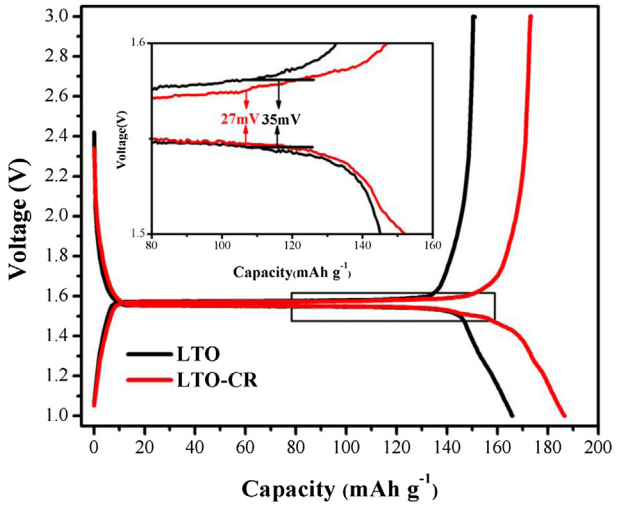

Fig. 5. Charge–discharge curves of LTO and LTO-CR, with the inset showing a magnification of the indicated region.

indicating that the polarization of the LTO-CR electrode is suppressed by the CeO_2 coating [43].

Fig. 6 displays the discharge capacity vs. cycle number and coulombic efficiency for LTO and LTO-CR between 1.0 and 3.0 V at 10 C. LTO-CR exhibits an excellent discharge capability (152 mAh g^{-1}) with no obvious capacity fading up to 180 cycles, which is much higher than that of LTO at 119 mAh g^{-1}. In addition, the coulombic efficiency of both samples is similar, initial coulombic efficiency of LTO-CR (99%) at 10 C is higher than that of LTO (98%), which indicated that CeO_2 coating reduces the polarization of the LTO-CR electrode. The samples keep high coulombic efficiency (~ 100%) at all cycling, due to $Li_4Ti_5O_{12}$ is SEI free material during charge–discharge above 1.0 V [8,16], indicating that the electrochemical process of Li^+ insertion/desertion is reversible even at high current density [29]. The significant improvement in electrochemical performance of the LTO-CR electrode can be attributed to the improvement of electrical conductivity and lithium ion diffusion through the CeO_2 coating.

Furthermore, the LTO-CR exhibits better rate performance compared to LTO. The cells were progressively charged and discharged in a series of stages with increasing current rate from 0.2 to 40 C. As shown in Fig. 7, the capacity of LTO decreases dramatically above 20 C, while the capacity of the LTO-CR electrode decreases much more slowly at the same rate. Remarkably, LTO-CR can deliver a specific capacity of 128.4 mAh g^{-1} at 40 C, while LTO displays the specific capacity of 79.7 mAh g^{-1}. The rate performance of LTO-CR is much better compared to the reported data [15,25,28,29]. The

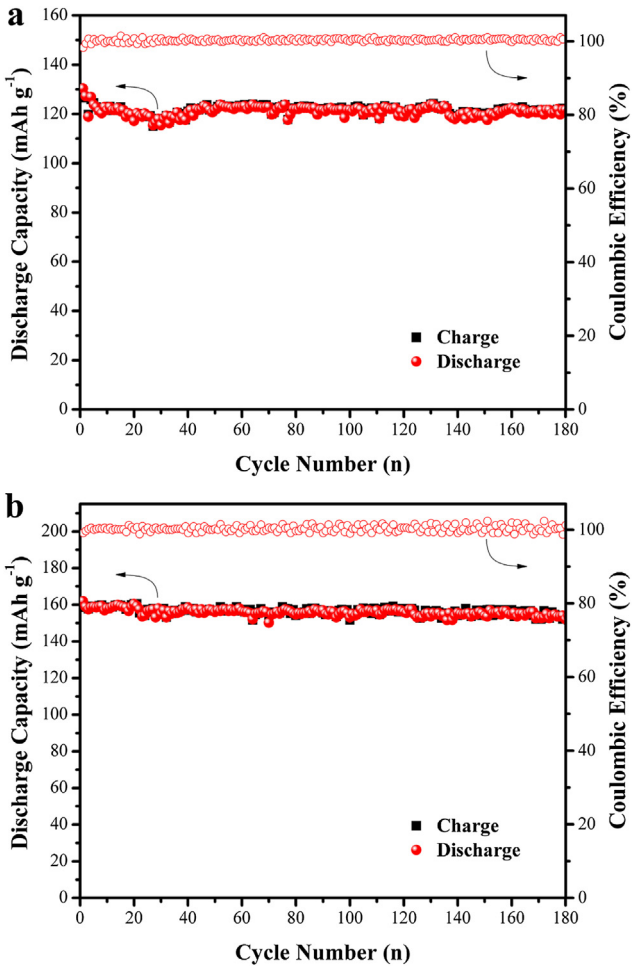

Fig. 6. Cycling performance and coulombic efficiency of (a) LTO and (b) LTO-CR at 10 C.

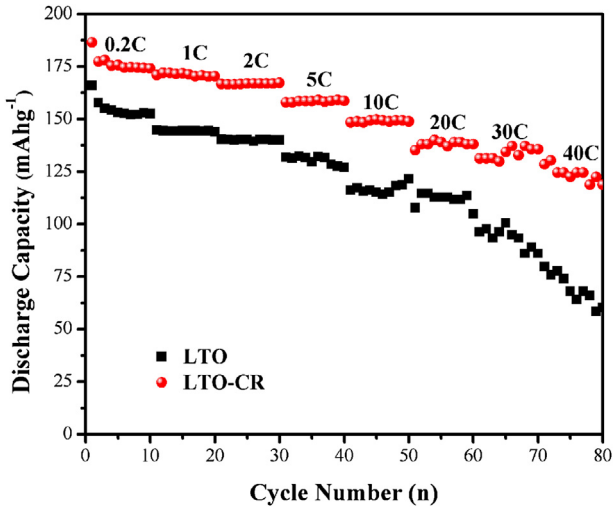

Fig. 7. Rate performance of LTO and LTO-CR.

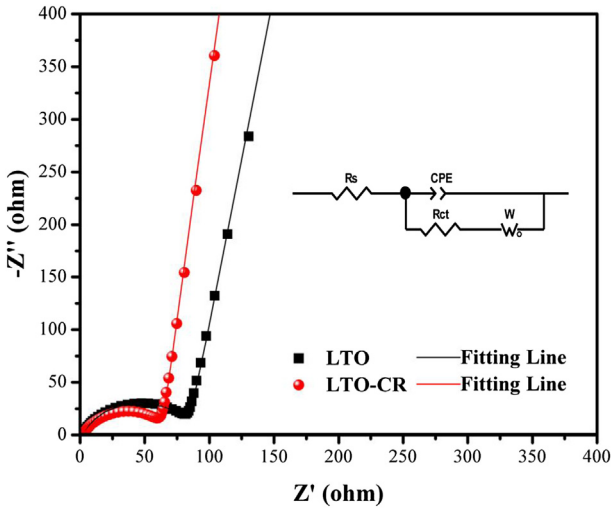

Fig. 8. Electrochemical impedance spectra of LTO and LTO-CR, with the inset showing equivalent circuit model used for the fitting.

$Li_4Ti_{5-x}W_xO_{12}$ ($x = 0, 0.05, 0.1, 0.15$ and 0.2) prepared by Zhang et al. [15] presented a discharge capacity of 110.4 mAh g^{-1} at 20 C. Shen et al. [25] designed and fabricated self-supported $Li_4Ti_5O_{12}$ nanowires that exhibited 121 mAh g^{-1} at 30 C. Zhu et al. [28] reported the synthesis of carbon coated nanosized $Li_4Ti_5O_{12}$, which showed a specific capacity of 126 mAh g^{-1} at 20 C. The N-doped carbon coated $Li_4Ti_5O_{12}$ fabricated by Li et al. [29] exhibited a discharge capacity of 123 mAh g^{-1} at 30 C. Compared to the published results, the electrochemical performance of LTO-CR is even better, indicating that CeO_2 coating could be a simple and effective way to improve the rate performance of LTO electrodes, and the CeO_2 coating can significantly improve the electrochemical kinetics of LTO-CR electrodes.

The much improved electrochemical performance of the LTO-CR could be explained as follows: Firstly, TEM data shows that the CeO_2 coating layer prevents aggregation between active particles, facilitating formation of LTO-CR nanoparticle, the electrolyte can permeate easily, which will accelerate the electrochemistry reaction. Interestingly, LTO-CR shows excellent rate performance because nanostructure can improve kinetic performance [28,44]. What's more, spherical morphology also improves the electrode performance owing to the length of the diffusion pathway is significantly shortened [39]. Secondly, CeO_2 has good electrical conductivity, which enhances the total electrical conductivity of the LTO-CR composite electrodes. In addition, the CeO_2 coating layer can restrain the resistance increase during the charge–discharge process [32]. Thirdly, Rietveld analysis of XRD data illustrates the partial doping of Ce^{4+} into the $Li_4Ti_5O_{12}$ structure may enhance lithium diffusivity and facilitate charge transfer reactions, especially at high current densities.

To clarify the effects of the CeO_2 coating on the electrochemical properties of $Li_4Ti_5O_{12}$, the resistance and the electrochemical reaction properties of the electrodes were further measured by EIS, as shown in Fig. 8. The two Nyquist plots consist of one high to medium frequency semicircle and one low frequency straight line. The high to medium frequency semicircle is mainly related to the charge transfer resistance [45]. The low frequency straight line indicates the Warburg impedance caused by Li^+ diffusion within the electrode material [12,21,44]. The EIS are fitted using the equivalent circuit shown in the inset of Fig. 8. In this equivalent circuit, R_s and R_{ct} are the resistance of electrolyte [15,19,37,44] and the charge transfer resistance [15], respectively; CPE reflects the interfacial capacitance [14]; W represents the Warburg impedance. R_{ct} relies on the electronic and ionic conductivity [46]. The fitted results of as-prepared materials by EIS are tabulated in Table 1. Apparently, the charge transfer resistance of LTO-CR is smaller, which is beneficial for the enhancement of the conductivity and the kinetic behavior [15].

To further confirm this result, the lithium ion diffusion coefficient is calculated by the following equation [14,16,47,48].

$$D = \frac{R^2T^2}{2An^4F^4C^2\sigma^2} \quad (1)$$

$$Z_{re} = R_s + R_{ct} + \sigma\omega^{-0.5} \quad (2)$$

where D is Li^+ diffusion coefficient, T is the room temperature (298 K), R is the gas constant (8.314 J mol^{-1} K^{-1}), A is the surface area of the electrode (1.13 cm^2), n is the number of electrons during in the half-reaction of the redox couple (equal to 1) [48], F is the Faraday constant (96500 C mol^{-1}), C is molar concentration of Li^+ in solid (4.37×10^{-3} mol cm^{-3}) [48], ω is the angular frequency, and σ is the Warburg impedance coefficient, which is relative to Z_{re} (real part of the impedance) through Equation (2). And the value of σ can be calculated from the slope of the lines between Z_{re} and $\omega^{-0.5}$ in Fig. 9. The Li^+ diffusion coefficient values are given in Table 1, where we can find that LTO-CR has larger Li^+ diffusion coefficient than LTO. In summary, the $Li_4Ti_5O_{12}$@CeO_2 nanosphere enhance Li^+ diffusion coefficient and facilitate the charge transfer reactions during charge–discharge process, with both of these positive effects contributing to the improved electrochemical performance of LTO-CR electrode compared to LTO.

4. Conclusions

Core–shell $Li_4Ti_5O_{12}$@CeO_2 nanosphere was successfully synthesized by a facile one-pot co-precipitation method. The $Li_4Ti_5O_{12}$@CeO_2 nanosphere exhibits excellent cycling stability at

Table 1
Fitted results of as-prepared materials by EIS.

Samples	R_s (Ω)	R_{ct} (Ω)	σ (Ω $s^{-0.5}$)	D (cm^2 s^{-1})
LTO	2.74	76.67	162.11	5.52×10^{-14}
LTO-CR	2.39	60.81	103.53	1.35×10^{-13}

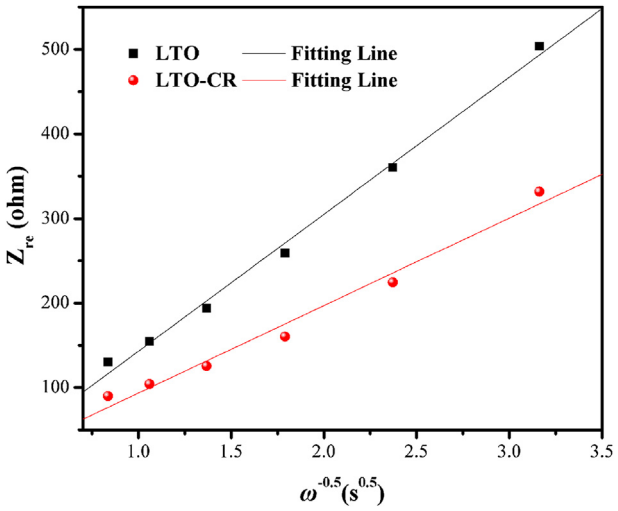

Fig. 9. Real parts of the complex impedance versus $\omega^{-0.5}$ at low frequency region for LTO and LTO-CR.

the high rate of 10 C and outstanding rate performance as anode material for lithium-ion batteries. The results demonstrate the feasibility of CeO_2 as an alternative coating to improve the electrochemical performance of $Li_4Ti_5O_{12}$ at high current density. The present synthesis technique for the $Li_4Ti_5O_{12}$@CeO_2 composite, compared to the commonly applied complicated coating procedures, would have great potential in future mass production.

Acknowledgments

This work was supported by the Nature Science Foundation of Xinjiang Province (2013211A004), the Program for New Century Excellent Talents in University (NCET-12-1076), the National Natural Science Foundation of China (21161021) and the Program for Changjiang Scholars and Innovative Research Team in University of Ministry of Education of China (No. IRT1081).

References

[1] J.M. Tarascon, M. Armand, Nature 414 (2001) 359–367.
[2] H. Yan, Z. Zhu, D. Zhang, W. Li, Qilu, J. Power Sources 219 (2012) 45–51.
[3] H.L. Wu, Y.D. Huang, D.Z. Jia, Z.P. Guo, M. Miao, J. Nanopart. Res. 14 (2012) 713–719.
[4] K. Zaghib, M. Simoneau, M. Armand, M. Gauthier, J. Power Sources 81–82 (1999) 300–305.
[5] L. Zhao, Y.S. Hu, H. Li, Z. Wang, L. Chen, Adv. Mater. 23 (2011) 1385–1388.
[6] Z.Y. Wen, Z.H. Gu, S.H. Huang, J.H. Yang, Z.X. Lin, O. Yamamoto, J. Power Sources 146 (2005) 670–673.
[7] T. Ohzuku, A. Ueda, N. Yamamota, J. Electrochem. Soc. 142 (1995) 1431–1435.
[8] T.-F. Yi, Y. Xie, Y.-R. Zhu, R.-S. Zhu, H. Shen, J. Power Sources 222 (2013) 448–454.
[9] F. Wu, X. Li, Z. Wang, H. Guo, Nanoscale 5 (2013) 6936–6943.
[10] Y. Huang, Y. Qi, D. Jia, X. Wang, Z. Guo, W.I. Cho, J. Solid State Electrochem. 16 (2011) 2011–2016.
[11] S.H. Huang, Z.Y. Wen, X.J. Zhu, Z.H. Gu, Electrochem. Commun. 6 (2004) 1093–1097.
[12] T.F. Yi, Y. Xie, Q.J. Wu, H.P. Liu, L.J. Jiang, M.F. Ye, R.S. Zhu, J. Power Sources 214 (2012) 220–226.
[13] Y.J. Bai, C. Gong, N. Lun, Y.X. Qi, J. Mater. Chem. A 1 (2013) 89–96.
[14] C.F. Lin, M.O. Lai, L. Lu, H.H. Zhou, Y.L. Xin, J. Power Sources 244 (2013) 272–279.
[15] Q.Y. Zhang, C.L. Zhang, B. Li, D.D. Jiang, S.F. Kang, X. Li, Y.G. Wang, Electrochim. Acta 107 (2013) 139–146.
[16] T.-F. Yi, S.-Y. Yang, X.-Y. Li, J.-H. Yao, Y.-R. Zhu, R.-S. Zhu, J. Power Sources 246 (2014) 505–511.
[17] B. Zhang, H. Du, B. Li, F. Kang, Electrochem. Solid-State Lett. 13 (2010) A36–A38.
[18] P. Kubiak, A. Garcia, M. Womes, L. Aldon, J. Olivier-Fourcade, P.E. Lippens, J.C. Jumas, J. Power Sources 119 (2003) 626–630.
[19] B.B. Tian, H.F. Xiang, L. Zhang, Z. Li, H.H. Wang, Electrochim. Acta 55 (2010) 5453–5458.
[20] T.-F. Yi, Y. Xie, L.-J. Jiang, J. Shu, C.-B. Yue, A.-N. Zhou, M.-F. Ye, RSC Adv. 2 (2012) 3541–3547.
[21] Y.R. Jhan, J.G. Duh, Electrochim. Acta 63 (2012) 9–15.
[22] D.H. Kim, Y.S. Ahn, J. Kim, Electrochem. Commun. 7 (2005) 1340–1344.
[23] Y.F. Tang, L. Yang, Z. Qiu, J.S. Huang, Electrochem. Commun. 10 (2008) 1513–1516.
[24] A.S. Prakash, P. Manikandan, K. Ramesha, M. Sathiya, J.M. Tarascon, A.K. Shukla, Chem. Mater. 22 (2010) 2857–2863.
[25] L. Shen, E. Uchaker, X. Zhang, G. Cao, Adv. Mater. 24 (2012) 6502–6506.
[26] Y.Q. Wang, L. Gu, Y.G. Guo, H. Li, X.Q. He, S. Tsukimoto, Y. Ikuhara, L.J. Wan, J. Am. Chem. Soc. 134 (2012) 7874–7879.
[27] L. Cheng, J. Yan, G.N. Zhu, J.Y. Luo, C.X. Wang, Y.Y. Xia, J. Mater. Chem. 20 (2010) 595–602.
[28] G.N. Zhu, H.J. Liu, J.H. Zhuang, C.X. Wang, Y.G. Wang, Y.Y. Xia, Energy Environ. Sci. 4 (2011) 4016–4022.
[29] H.S. Li, L.F. Shen, K.B. Yin, J. Ji, J. Wang, X.Y. Wang, X.G. Zhang, J. Mater. Chem. A 1 (2013) 7270–7276.
[30] G. Wang, J.T. Bai, Y.H. Wang, Z.Y. Ren, J.B. Bai, Scr. Mater. 65 (2011) 339–342.
[31] Q.M. Su, L. Chang, J. Zhang, G.H. Du, B.S. Xu, J. Phys. Chem. C 117 (2013) 4292–4298.
[32] D. Arumugam, G.P. Kalaignan, Electrochim. Acta 55 (2010) 8709–8716.
[33] F. Zhou, X.M. Zhao, H. Xu, C.G. Yuan, J. Phys. Chem. C 111 (2007) 1651–1657.
[34] H.W. Ha, N.J. Yun, M.H. Kim, M.H. Woo, K. Kim, Electrochim. Acta 51 (2006) 3297–3302.
[35] H.W. Ha, N.J. Yun, K. Kim, Electrochim. Acta 52 (2007) 3236–3241.
[36] B. Hunter, International Union of Crystallography Commission on Powder Diffraction Newsletter No. 20 (Summer), 1998, http://www.rietica.org.
[37] Z. Liu, N. Zhang, K. Sun, J. Mater. Chem. 22 (2012) 11688–11693.
[38] W.K. Pang, N. Sharma, V.K. Peterson, J.-J. Shiu, S.-H. Wu, J. Power Sources 246 (2014) 464–472.
[39] L. Shen, C. Yuan, H. Luo, X. Zhang, K. Xu, Y. Xia, J. Mater. Chem. 20 (2010) 6998–7004.
[40] J. Haetge, P. Hartmann, K. Brezesinski, J. Janek, T. Brezesinski, Chem. Mater. 23 (2011) 4384–4393.
[41] Y. Qi, Y. Huang, D. Jia, S.-J. Bao, Z.P. Guo, Electrochim. Acta 54 (2009) 4772–4776.
[42] C.X. Hua, X.P. Fang, Z.W. Yang, Y.R. Gao, Z.X. Wang, L.Q. Chen, Electrochem. Commun. 25 (2012) 66–69.
[43] H.F. Ni, L.Z. Fan, J. Power Sources 214 (2012) 195–199.
[44] W.L. Zhang, J.F. Li, Y.B. Guan, Y. Jin, W.T. Zhu, X. Guo, X.P. Qiu, J. Power Sources 243 (2013) 661–667.
[45] X. Li, C. Lai, C.W. Xiao, X.P. Gao, Electrochim. Acta 56 (2011) 9152–9158.
[46] B.H. Li, C.P. Han, Y.B. He, C. Yang, H.D. Du, Q.H. Yang, F.Y. Kang, Energy Environ. Sci. 5 (2012) 9595–9602.
[47] N. Takami, A. Satoh, M. Hara, T. Ohsaki, J. Electrochem. Soc. 142 (1995) 371–378.
[48] S.-L. Chou, J.-Z. Wang, H.-K. Liu, S.-X. Dou, J. Phys. Chem. C 115 (2011) 16220–16227.